

of the still unknown parameters, increasing the number of constraints of the model.

For the arclets or the weakly magnified galaxies which are too faint to be observed spectroscopically, we also expect some progress by using multi-colour photometric data spread over a large spectral range, such as B, R and I colours. In that case we can compare the colour indices of the objects with the predictions of spectrophotometric models of galaxy evolution, in order to evaluate a "photometric redshift". This method is being calibrated with the known arcs, and we are conscious that it is only useful in a statistical way, when a large number of arclets is being observed. The preliminary results of the method, applied in the field of A370 show that most of the galaxies have colours compatible with galaxies at redshift around 1, reinforcing the results presented above (Fort et al., in preparation).

Last but not least, in a few optimal cases, we expect to get a complete set of data in some clusters: high-resolution X-ray map with ROSAT, multiple arcs and a lot of arclets and weakly distorted images of background galaxies for a reconstruction of the 2D gravitational potential of the Dark Matter from the centre to the external radius of the cluster. The redshift of the giant arcs is in this case fundamental in order to fix the scaling of the potential in the lens modellings.

The use of the gravitational telescope for the study of distant galaxies appears to be a powerful and original tool, which is probably not yet fully used. For example, we can also expect to find some "exotic" magnified objects, such as very distant quasars (La Borgne et al., 1990) or we hope to "see" some spatial structures in galaxies at $z = 1$ through the distortion of the clusters. The arc survey opened for us a new window in the $z = 1$ Universe!

Acknowledgements

I wish to thank all my colleagues from the Toulouse-Barcelona group, namely B. Fort, H. Bonnet, J.P. Kneib, J.F. LeBorgne, G. Mathez, Y. Mellier, R. Pelló, J.P. Picat and B. Sanahuja with whom I have worked on arcs and lenses for many years in such a friendly environment! Also many thanks to our collaborators T. Tyson (Bell Labs), G. Bernstein (Tucson), R. Ellis, M. Fitchett and I. Smail from Durham for all the data provided and the exciting discussions we had about observations of gravitational lenses.

References

Bruzual G., Charlot S., 1992, submitted to *Ap.J.*
Cowie L.L., Songaila A., Hu E.M., 1991, *Nature* **354**, 460.

Guiderdoni, B., Rocca-Volmerange B., 1987, *A & A* **186**, 1.
Ellis R.S., Allington-Smith, J.R., Smail I., 1991, *M.N.R.A.S.* **249**, 184.
Fort B., Prieur J.L., Mathez G., Mellier Y., Soucail G., 1988, *A & A* **200**, L17.
Fort B., Le Borgne J.F., Mathez G., Mellier Y., Picat J.P. Soucail G., Pelló R., Sanahuja B., 1990, *The Messenger* **62**, 11.
Fort B., Le Fèvre O., Hammer F., Cailloux M., 1992, *Ap.J.*, submitted.
Kassiola A., Kovner I., Blandford R.D., 1992, *Ap.J.*, in press.
Kassiola A., Kovner I., Fort B., 1992, *Ap.J.* in press.
Lynds R., Petrosian V., 1986, *B.A.A.S.*, **18**, 1014.
Le Borgne J.F., Pelló R., Sanahuja B., Soucail G., Mellier Y., Breare M., 1990, *A & A* **229**, L13.
Mellier Y., Fort B., Soucail G., Mathez G., Cailloux M., 1991, *Ap.J.* **380**, 334.
Mellier Y., Fort B., Kneib J.P., 1992, *Ap.J.*, in press.
Pelló R., Le Borgne J.F., Soucail G., Mellier Y., Sanahuja B., 1991, *Ap.J.* **366**, 405.
Pelló R., Le Borgne J.F., Sanahuja B., Mathez G., Fort B., 1992, *A & A*, submitted.
Smail I., Ellis R.S., Aragón-Salamanca A., Soucail G., Mellier Y., Giraud E., 1992, *M.N.R.A.S.*, in press.
Soucail G., Fort B., Mellier Y., Picat J.P., 1987, *A & A* **172**, L14.
Soucail G., Mellier Y., Fort B., Mathez G., Cailloux M., 1988, *A & A* **191**, L19.
Soucail G., Fort B., 1991, *A & A* **243**, 23.
Tyson J.A., 1988, *A.J.* **96**, 1.
Tyson J.A., Valdes F., Wenk R.A., 1990, *Ap.J.* **349**, L1.

Quasar Absorption Spectra: The Physical State of the Intergalactic Medium at High Redshifts

E. GIALLONGO, Osservatorio Astronomico di Roma, Monteporzio, Italy

S. CRISTIANI, Dipartimento di Astronomia, Università di Padova, Italy

A. FONTANA, Dipartimento di Fisica, Il Università di Roma, Italy

D. TRÈVESE, Istituto Astronomico, Università di Roma "La Sapienza", Italy

1. Introduction

An important source of information on the distribution and the physical state of the intergalactic medium (IGM) up to redshift $z \approx 5$ is provided by the study of the absorption spectra of high redshift quasars. The crowd of narrow absorption lines seen shortward of the QSO Lyman- α emission is thought to be due mainly to Lyman- α absorptions caused by intervening clouds along the line-of-sight (Lynds 1971; Sargent et al. 1980).

Direct measures of column densities and doppler widths of the absorption

lines provide typical values of $N_{\text{HI}} = 10^{14}$ atoms cm^{-2} and $b = \sqrt{2}\sigma = 20-30$ km s^{-1} (Carswell et al. 1987, 1991) correspondent to $T_c \sim 2-5 \times 10^4$ K, assuming thermal broadening. However, Pettini et al. (1990) claim typical b values as low as $b = 17$ km s^{-1} and a tight correlation between b and N_{HI} parameters which suggests lower temperatures and would imply a further important constraint on the physics of the clouds. More data are necessary to resolve this controversy.

The most recent and accurate esti-

mate of the cloud sizes has been obtained by Smette et al. (1991) from the spectra of a gravitationally lensed high-redshift quasar UM673 ($z_{\text{em}} = 2.7$). They derive lower and upper limits of $12h_{50}^{-1}$ kpc and $160h_{50}^{-1}$ kpc respectively, for the diameter of spherical clouds, or 24 kpc and 320 kpc, for oblate spheroids with an axis ratio < 0.1 .

Under these conditions, gravitational energy is overwhelmed by thermal energy and the clouds could be confined by a hotter, highly ionized and diffuse IGM if non-baryonic dark matter does not

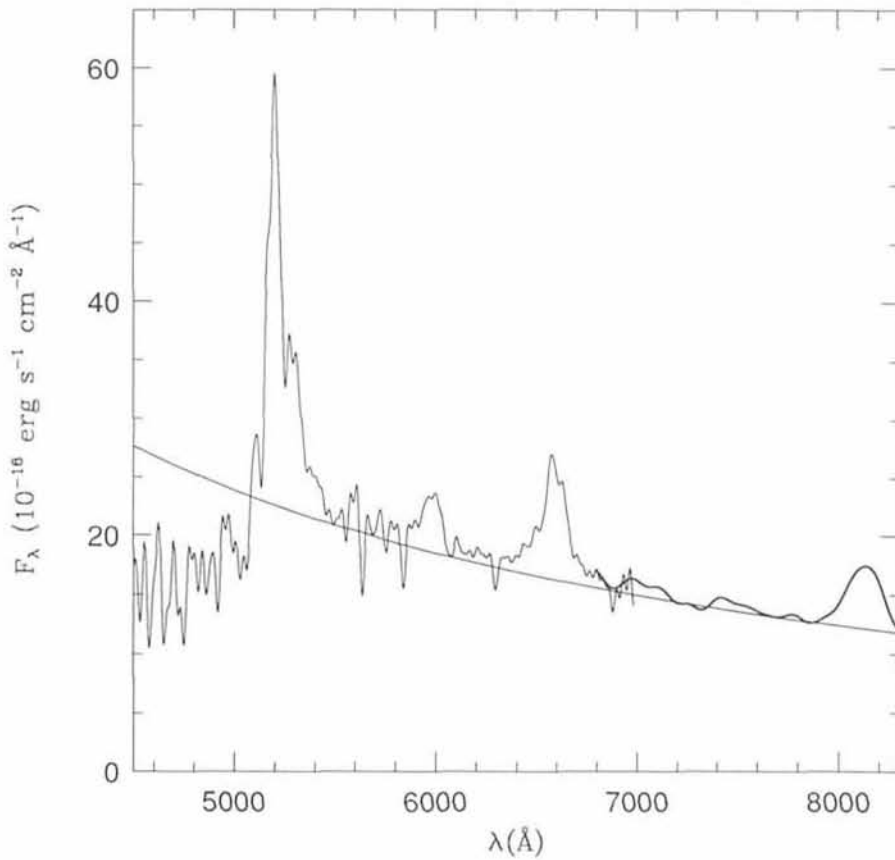


Figure 1: Composite spectrum of Q2126-158. High-resolution data are smoothed to 10 \AA resolution. Thick curve represents the low-resolution data. The fitted continuum is also shown.

quasar absorption spectra particularly suitable to investigate the physical properties of the diffuse and clumpy components of the IGM.

As an example, we present a high resolution spectrum ($R = 22,000$) of the quasar Q2126-158 at $z = 3.27$, extending from 4500 to 7000 \AA , and show how we can extract crucial information like the density of the diffuse neutral hydrogen and the distribution of density and temperature of the Lyman- α clouds.

2. Data Acquisition and Reduction

The quasar Q2126-158 was observed at ESO (La Silla) in August 1991, with the NTT telescope and the EMMI instrument in the echelle mode (see D'Odorico 1990). Two spectra of 7200 s each were obtained on August 6, and one of 9130 s on August 7. The slit was 1.5 arc-seconds wide and the seeing always less or equal to 1 arcsec. Particular attention was paid in order to minimize the effects of the atmospheric dispersion. The absolute flux calibration was carried out by observing the standard star EG274. The data reduction has been carried out using the standard echelle package described in the 91NOV edition of the MIDAS software (Banse et al. 1983). The weighted mean

contribute appreciably to the gravitational potential of the clouds (see however Rees 1986).

The ionization of the IGM can be constrained by the absence of the long looked-for absorption trough shortward of the QSO Lyman- α emission, with the average optical depth $\tau_{\text{GP}} \leq 0.5$, (GP test, see Gunn and Peterson 1965).

Considering that the background ionizing UV flux produced by the quasar population at $z = 2-3$, $J = 10^{-22} \text{ J}_{-22} \text{ ergs cm}^{-2} \text{ s}^{-1} \text{ Hz}^{-1} \text{ sr}^{-1}$ (Madau 1992), keeps both the clouds and IGM ionized, the physical state and evolution of the diffuse IGM can be further constrained under the assumption that clouds are pressure confined (Sargent et al. 1980, Ostriker and Ikeuchi 1983, Steidel and Sargent 1987). Taken together, the above conditions define a region in the density-temperature plane which provides an upper limit to the IGM baryon density Ω_{IGM} which can give information about the efficiency of the galaxy formation processes.

High resolution spectroscopy available with good efficiency over a large spectral range, using the EMMI instrument at the NTT telescope, will allow to collect a homogeneous sample of

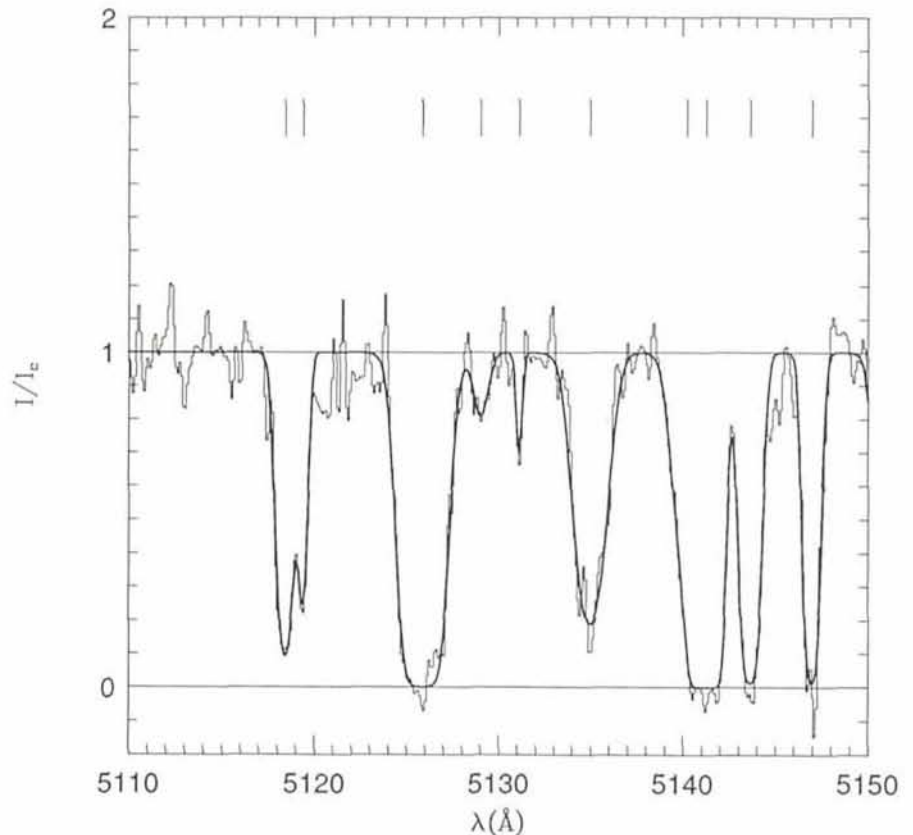


Figure 2: A selected region in the Ly- α forest, with the fitted profiles.

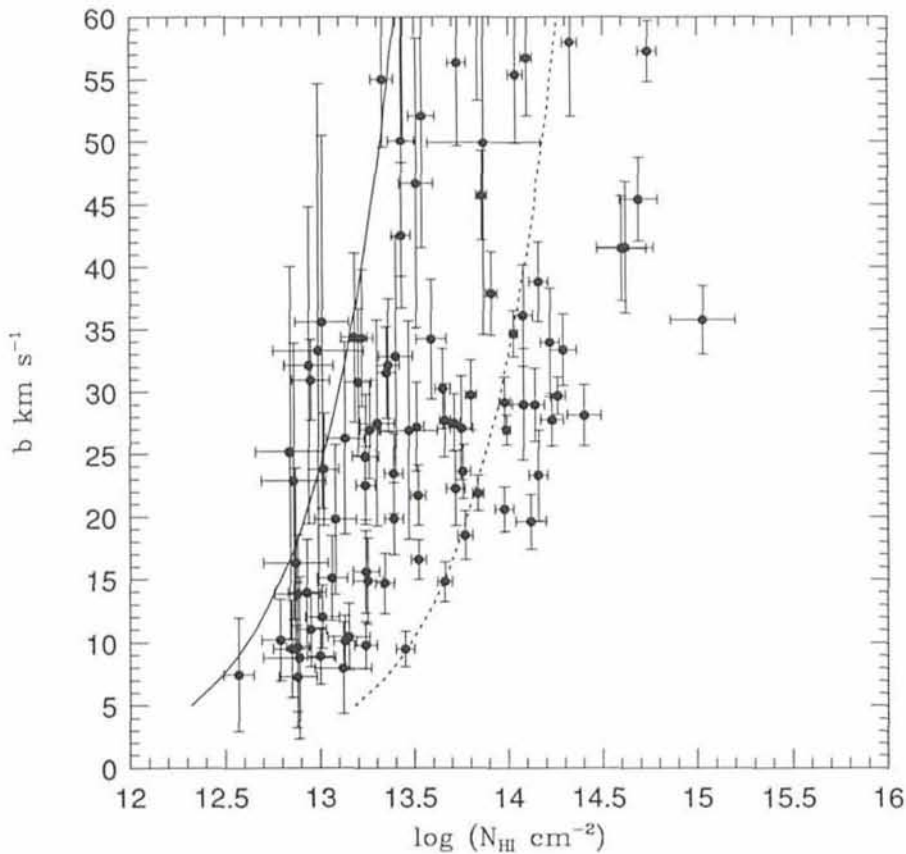


Figure 3: Velocity-dispersion parameter b versus the logarithm of the neutral hydrogen column density $\log N_{\text{HII}}$ of Ly- α lines. The continuous curve represents our selection criterion. The dashed curve corresponds to a central flux of 0.1 where the noise level becomes comparable to the signal and lines start to saturate.

of the spectra has been obtained at the resolution $R = 22,000$ and is shown in Figure 1 smoothed to $\sim 10 \text{ \AA}$ for illustrative purpose. The S/N ratio ranges from 6 to 12 in the Ly- α forest region.

Q2126-158 had previously been observed by us at low resolution ($\sim 25 \text{ \AA}$), using the B & C spectrograph at the 2.2-m ESO/MPI telescope at La Silla on September 3, 1989. Two exposures of 30 min each were taken with a 5 arcsec wide slit in the spectral range 3300-8650 \AA . A standard reduction was carried out with the long-slit package of MIDAS. The absolute flux calibration was obtained observing the standard star LDS 749B.

The two spectra have then been compared, finding that, apart from the difference of a factor 100 in resolution and a renormalization factor close to unity, there was a perfect correspondence within the noise. The red part $\lambda > 7000 \text{ \AA}$ of the low-resolution spectrum has then been appended (after renormalization) to the echelle spectrum as shown in Figure 1.

3. The Quasar Continuum and the Gunn-Peterson Test

The total opacity in the Lyman- α forest is given by the sum of the line

contribution and the GP opacity due to diffuse hydrogen absorption: $\tau = \tau_{\text{GP}} + \tau_{\text{l}}$, and can be measured once the quasar continuum has been established.

From composite quasar spectra and from Figure 1 it can be shown that there are few regions which can be assumed as representative of the true continuum level. The region between Ly α and CIV emissions is affected by the presence of weak emission lines whose broad wings tend to overlap (OI 1302, CII 1335, SiIV 1400) and the region between CIV and CIII] emissions is affected by HeII 1640 and OIII] 1663 and by the blue end of the blended FeII 2000 complex. With this caution the fitted power-law is shown in Figure 1 ($\alpha_{\nu} = -0.62$).

At this point, regions free of strong absorption lines, where the r.m.s. fluctuation about the mean flux becomes consistent with noise statistics, are selected to estimate the GP depression. The power-law continuum estimated longward of Ly α emission is extrapolated in the Lyman- α forest and compared with the local continuum level of the selected regions. We obtain an average opacity at $z = 3$ of $\tau_{\text{GP}} = 0.013 \pm 0.026$. This new value of the hydrogen opacity can be used to constrain density and temperature of the IGM supposed to be ionized by the UV flux of quasars at $z = 3$. For

example, adopting ionization equilibrium with $J_{-22} = 1$ and an IGM temperature of $T_{\text{IGM}} \leq 2 \times 10^4 \text{ K}$ at $z = 3$ we find $\Omega_{\text{IGM}} = 0.006 - 0.013$ for our best fit and 1σ GP estimate respectively (Giallongo, Cristiani and Trèvese 1992).

This is the first direct measure of the GP opacity carried out using high-resolution quasar spectra with good relative flux calibration as can be obtained from the NTT+EMMI echelle-mode configuration.

4. Properties of the Lyman Alpha Absorption Lines

Quasar absorption spectra at a resolution $R > 20,000$ allow a direct determination of the column density and of the doppler parameter b through line profile fitting.

The line detection is performed in the following way. In regions of the Ly α forest with uniform signal-to-noise we construct the histogram of the pixel intensities. In general, because of absorption line contamination in the normalized spectrum, the distribution is not symmetrical in the Ly α forest but is skewed towards lower intensity values. We fit a Gaussian profile to the high intensity side of the histogram starting from the maximum of the intensity distribution: the variance obtained is taken as a conservative estimate of the noise level in the region considered. All the lines whose central relative intensity is less than $(1 - 2\sigma)$ are selected to form a complete sample. It is clear that a threshold of this type corresponds to a well-defined locus in the $b - \log N_{\text{HII}}$ plane (b is in km s^{-1} and N_{HII} in cm^{-2}).

The usual χ^2 fitting procedure is adopted to deblend the line profiles (Carswell et al. 1987, 1991). The number of components is assumed as the minimum which gives a probability of random deviation $P > 0.05$. An example of the resulting profiles is shown in Figure 2. In general this objective procedure is satisfactory though, in some cases, lines with a small number of pixels and poor S/N ratio are classified as single although they clearly appear as double from visual inspection.

After removing metal line systems, which are easily identified through the observation of the CIV doublet seen longward of the QSO Ly α emission, we obtain, in the region from 4750 to 5200 \AA , a complete sample of Ly α lines whose distribution in the $b - \log N_{\text{HII}}$ plane is shown in Figure 3. Two curves of constant central line flux containing most of the sample are also represented. The upper envelope represents our selection criterion: lines with central flux less than the threshold are included in the complete sample. The

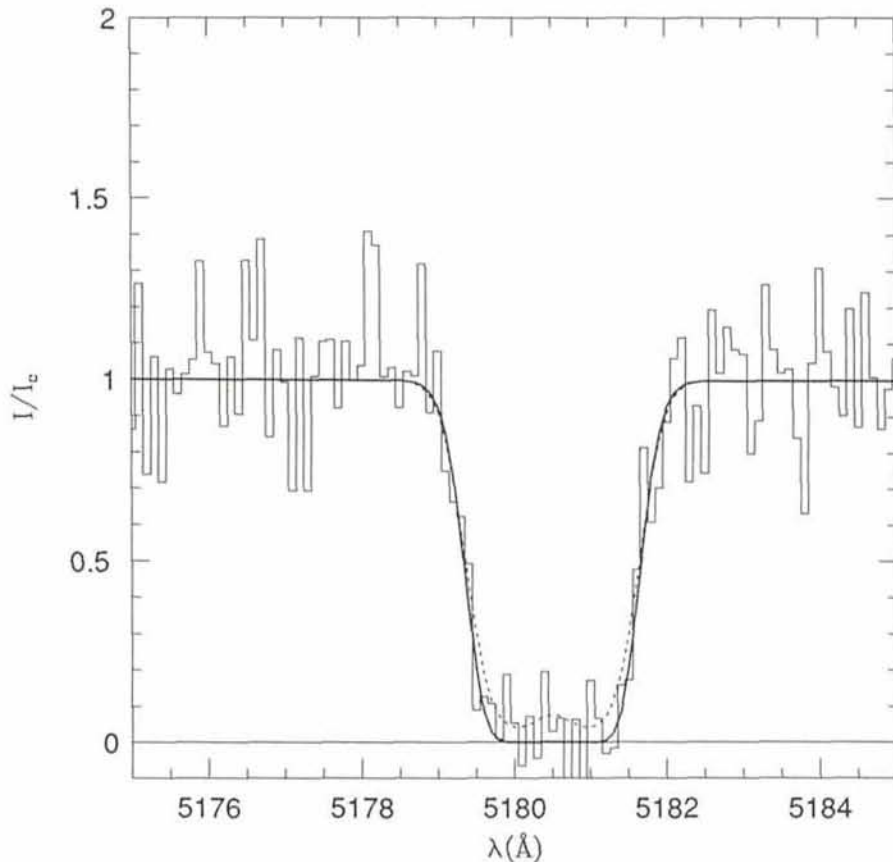


Figure 4: Simulated blend of two lines with $b = 30$, $\log N_{\text{HI}} = 14.1$, separated by 1 \AA , with $S/N = 6$. Dotted curve: profile of the individual components. Continuous curve: single line fitted profile, with $b = 35$ and $\log N_{\text{HI}} = 15.1$.

lower curve corresponds to a central flux of 0.1 where the noise level becomes comparable to the signal and lines start to saturate, in the range of b considered: lines on the right of this curve could be unresolved blends. It is clear that unsaturated lines show a tight correlation which reflects the selection effects (line-selection + non-saturation). However, the saturated lines, which are clearly identified in our spectrum, are

not uniformly distributed in the same range of b occupied by unsaturated lines. In particular, the absence of clearly single lines with $b < 20$ and $\log N_{\text{HI}} > 13.5$ is not due to any bias. Moreover, almost all the saturated features appear as unresolved blends and the reality of lines with $\log N_{\text{HI}} > 14$ in our spectrum is cast in serious doubt. The same could be true for lines with $b > 35$.

According to this interpretation, most

of the lines which appear as saturated could be unresolved blends of unsaturated lines which should occupy the top ($b \geq 30$ and $\log N_{\text{HI}} \leq 14$) of the apparently correlated distribution, as can be seen in Figure 4 where a simulated blend of two lines with the above parameters and $S/N = 6$ has been fitted as a single line of $b = 35$ and $\log N_{\text{HI}} = 15.1$, comparable with the line of highest column density in our sample.

Thus blending plays a crucial role in the interpretation of the observations, as has been shown recently by Trèvese, Giallongo and Camurani (1992). However, increasing the signal-to-noise ratio would raise the upper curve in Figure 3 and move downwards the lower one and allow a better deblending. Thus, recognizing a possible intrinsic correlation between b and N_{HI} in the Lyman- α clouds is within the reach of the present ESO instrumentation.

References

- Banase, K. et al. 1983, "MIDAS" in *Proc. of DECUS*, Zurich, 87.
 Carswell, R.F. et al. 1987, *Ap.J.* **319**, 709.
 Carswell, R.F. et al. 1991, *Ap.J.* **371**, 36.
 D'Odorico, S. 1990, *The Messenger* **61**, 51.
 Giallongo, E., Cristiani, S. and Trèvese D. 1992, *Ap.J.L.* (in press).
 Gunn, J.E. and Peterson, B.A. 1965, *Ap.J.* **142**, 1633.
 Lynds, C.R. 1971, *Ap.J.* **164**, L73.
 Madau, P. 1992, *Ap.J.* **389**, L1.
 Ostriker, J.P. and Iveuchi, S. 1983, *Ap.J.* **268**, L63.
 Pettini, M. et al. 1990, *M.N.R.A.S.* **246**, 545.
 Rees 1986 *M.N.R.A.S.* **218**, 25P.
 Sargent, W.L.W. et al. 1980, *Ap.J.S.* **42**, 41.
 Smette, A. et al. 1992, *Ap.J.* **389**, 39.
 Steidel, C.C. and Sargent, W.L.W. 1987, *Ap.J.* **318**, L11.
 Trèvese D., Giallongo E., and Camurani L. 1992, *Ap.J.* (in press).

The Galaxy Population in Distant Clusters

A. BUZZONI¹, M. LONGHETTI^{1, 2}, E. MOLINARI¹ and G. CHINCARINI^{1, 2}

¹Osservatorio Astronomico di Brera, Milano, Italy; ²Università degli Studi, Milano, Italy

1. Introduction

Clusters of galaxies are recognized to be the basic building blocks tracing the large-scale structure in the Universe. Thanks to the large number of coeval objects all at the same distance we get more favourable statistics allowing to explore in much better detail the

evolutionary status of the galaxy population.

Moreover, it is relevant to clarify whether or not clusters are dynamically relaxed structures and how environmental conditions constrained galaxy formation among the different morphological types. We know for instance

that ellipticals always reside in high-density regions like the core of the clusters while spirals better trace the low-density peripheral regions (Dressler 1980).

Both the dynamical and photometric questions have much in common as environment conditions might have influ-